Evidence of Coulomb blockade behavior in a quasi-zero-dimensional quantum well on TiO_2 surface

Vincent Meunier[a,b], M. H. Pan[a], F. Moreau[b,c], K. T. Park[d], and E. W. Plummer[e,1]

[a]Center for Nanophase Materials Sciences, Oak Ridge National Laboratory, Oak Ridge, TN; [b]Computer Science and Mathematics Division, Oak Ridge National Laboratory, Oak Ridge, TN; [c]Physics Department, Facultés Universitaires Notre-Dame de la Paix, Namur, Belgium; [d]Physics Department, Baylor University, Waco, TX; and [e]Department of Physics and Astronomy, Louisiana State University, Baton Rouge, LA

Contributed by E. Ward Plummer, July 10, 2010 (sent for review December 6, 2009)

Line defects on the surface of rutile $TiO_2(110)$ form in pairs separated by 1.2 nm creating a quantum well. The well is effectively closed by the presence of two charged structures at both ends separated by a distance in the 10–20 nm range. As expected for quantum confinement a long period oscillatory feature of the local density of states is observed and attributed to the formation of discrete quantum states inside the system. It is at first glance surprising that the lowest energy quantum state of the well can be observed at room temperature. The properties of the quantum state cannot be explained in an independent-electron, band-like theory. Instead, electron-electron correlation must be included to give a satisfactory picture of the spatial distribution of the charge density. Theory predicts charging energies of 1.30 eV and 1.14 eV for quantum well lengths of 14 nm and 16 nm, respectively, in good agreement with a classical calculation and the size dependence of the capacitance. This observation opens up the possibility of experimentally imaging the transition from a Coulomb blockade localized in a zero-dimensional system to an independent-particle or band-like behavior in an extended one-dimensional system.

capacitor | Coulomb blockage | quantum confinement | titanium dioxide | scanning tunneling microscopy

One of the most striking features of quantum mechanics is the distinctive electronic behavior associated with each level of dimensionality. Advances in scanning probe techniques coupled with the ability to prepare low-dimensional systems of unprecedented quality permits the direct observation of a number of manifestations of quantum mechanics in dimensionally confined systems (1). For example, a recent study revealed the presence of one-dimensional electronic states in the region between self-organized metallic nanowires on a semiconducting surface (2), a textbook illustration of an electron in a one-dimensional box. The famous picture of electron waves in a quantum corral is another beautiful example of imaging the density distribution of electrons in quantum confining structures (3–5). The electronic behavior of such systems may often be successfully understood within the independent-electron picture. When dimensionality is further reduced from quasi one-dimension (Q1D) to quasi zero-dimension (Q0D), electron-electron correlations are increasingly important and, in some instances, even dominate. In that case, the single-electron picture breaks down. The failure of the single-electron description is exemplified by Coulomb blockade behavior (6, 7). Here, the presence of a net charge in the structure and the associated Coulomb repulsive potential hinder the addition of an extra electron. A convenient way to understand this behavior is through the concept of charging energy, similar to the energy stored on the plates of a conventional capacitor. For a typical spherical quantum well with tens of nanometer radius, the equivalent capacitance is on the order of the 10^{-17} F, which corresponds to a charging energy of the order of 10 meV. At sufficiently low temperatures, this energy is not readily available. Consequently, an electron cannot overcome the electrostatic barrier due to net charge present in the system.

Previously studied systems, such as the Q0D quantum corrals (3, 4) or the Q1D confinement by parallel platinum (Pt) nanowires on semiconductors (2), were associated with a significant amount of charge leakage, either because they were formed on metallic surfaces or because of the extended nature of the Q1D confinement. This electron leakage makes the concept of charging energy difficult to apply due to the screening of the Coulombic potential by bulk charges, thus preventing any comparison with the electron-electron repulsion energy in the different dimensional systems. But consider a system which exhibits strong confinement in two dimensions and weaker and variable confinement in the remaining dimension. The system could be tuned from the one-dimensional subband electronic structure of a Q1D system to the discrete-state electronic structure of Q0D system.

Coulomb blockade behavior at room temperature has been previously reported by Postma and coworkers in 2001 (8). Using an atomic force microscope, they measured charging energy of about 120 meV in a box made up of two local barriers into the single-wall carbon nanotube. Here we report on unique self-assembled nanostructures realized on $TiO_2(110)$, with estimated charging energies of more than 1 eV, about 10 times larger than that reported by Postma et al.. This large Coulomb charging energy is the result of the smaller size of the nanostructures shown here.

Results

Fig. 1*A* shows a system composed of two line defects (9) about 10 nm long and spaced 1.2 nm apart along the $[1\bar{1}0]$ direction. They are terminated with charged nanoclusters of TiO_2 forming what we call nanoclips. Inside of this Q0D structure is a periodic distortion with a period ~10 times the lattice spacing (Fig. 1*B*). This electronic wave is confined in the plane by the nanoclip and by the image potential and bulk band gap perpendicular to the surface (10, 11). The wave pattern is very reminiscent of the confined electron waves in the quantum corral (3, 4) or the one-dimensional wire (2, 5). However, we will show that this is not the correct picture, and strong electron-electron interaction is required to explain the experimental observations. This work opens up the possibility of preparing nanoclips with longer lengths thereby allowing the visualization of the transition from localized to band-like electronic structure.

The insert of Fig. 2*A* shows scanning tunneling microscope (STM) images of structures with three different lengths. The short one, $n = 0$ of length 6 nm, has no charge oscillation.

Author contributions: V.M., M.H.P., F.M., K.T.P., and E.W.P. designed research; V.M., M.H.P., F.M., and K.T.P. performed research; M.H.P. contributed new reagents/analytic tools; V.M., M.H.P., F.M., K.T.P., and E.W.P. analyzed data; and V.M., M.H.P., F.M., K.T.P., and E.W.P. wrote the paper.

The authors declare no conflict of interest.

Freely available online through the PNAS open access option.

[1]To whom correspondence should be addressed. E-mail: wplummer@phys.lsu.edu.

This article contains supporting information online at www.pnas.org/lookup/suppl/doi:10.1073/pnas.1009310107/-/DCSupplemental.

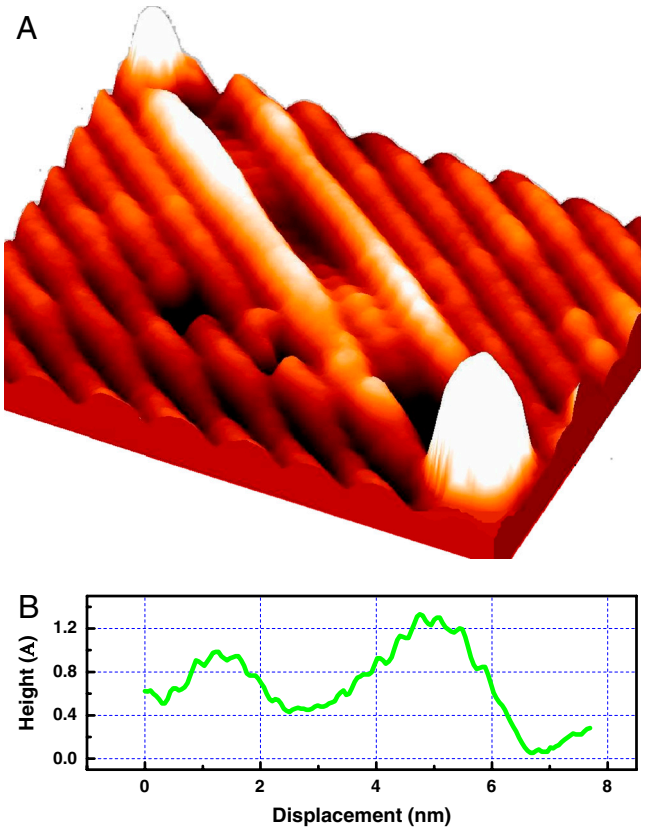

Fig. 1. (*A*) Constant-current, three-dimensional STM image of a 10 nm long "nanoclip" nanostructure on TiO_2 (110) substrate. A 3.8 nm period oscillation is observed, as shown on the line profile between the two ends of the linear nanoclip reproduced on (*B*).

The $n = 1$ structure is 16.5 nm long and shows one maximum and the $n = 2$ nanoclip is 17.5 nm long and exhibits two maxima.

The atomic structure of the single line defect has been fully determined using a combination of STM and density functional theory (9) and recently confirmed by transmission electron microscopy imaging (12). In each line defect, titanium (Ti) interstitials form the edge/face-sharing octahedra that serve as building blocks for (1×1) as well as (1×2) surface reconstructions on TiO_2 (110). In addition, the line defects are often terminated with bright spots at the ends. The height of an end feature is typically about twice that of the line defect, i.e., 3.2 Å above the 5-coordinated Ti (also referred to as "Ti^{4+}") row of the substrate. Furthermore, an end feature spans across both Ti^{4+} and bridging O (O_{br}) rows along (1–10). With the width along [1$\bar{1}$0] comparable to that along [001], the resulting shape is either oval or circular. These topographically distinctive dots have been interpreted as clusters of stoichiometric TiO_2. Detailed discussions on their structures and their roles in cluster nucleation and growth were presented elsewhere (13).

For the nanoclip in Fig. 2, the atomic structure of each sidewall is constructed using substoichiometric TiO_x ($x < 2$, in this case $x = 1$) units of edge/face-sharing octahedra. Each sidewall is connected to an end feature, made of two TiO_2 units in the repeating unit cell Fig. 2*B*. One TiO_2 unit has its molecular plane oriented horizontally to the surface above the 2-coordinate O_{br} while the other unit oriented vertically above the row of Ti^{4+} (highlighted with dotted oval). These two TiO_2 molecular units for an end feature represent the building blocks for stoichiometric surface regeneration via corner-sharing octahedra, as compared to the substoichiometric surface reconstruction by line defects. Previous experiments on surface dynamics showed that these dots played an active role as itinerant species in the restoration of oxygen-deficient TiO_2 (14–17). Upon exposure to oxygen, bright dots were observed to nucleate on terraces and subsequently converted into new terraces with line defects for layer-by-layer growth.

Typical STM images of the structures described above are shown in Fig. 2*A*. The manifestations of confinement are different in several notable ways compared to previously reported confinement in quantum corrals (3, 4). First the size of the confining box is approximately an order of magnitude smaller with a surface area of 1.2×20 nm^2, and its shape is more elongated than the typical oval corrals. Second, in addition to the long period modulation, the observed patterns also exhibit the intensity oscillation of a much shorter period corresponding to the 0.295 nm periodicity of the surface lattice along the [001] direction. Third, the substrate used here is essentially insulating with a large band

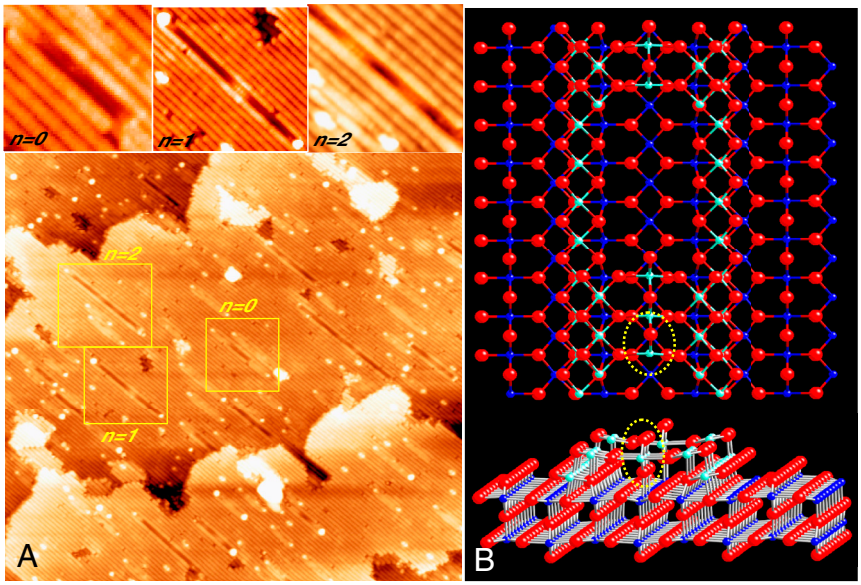

Fig. 2. (*A*) Constant current STM image for a large area scan (85×85 nm^2, 0.5 nA) exhibiting a number of double-line-defects (nanoclips), which show the observable charge oscillation inside. The insert figures focus on three different types of nanoclips: without charge oscillation ($n = 0$), with one maximum ($n = 1$) and with two maxima of oscillation ($n = 2$), respectively; (*B*) Ball-and-stick structural model of a typical "nanoclip" viewed from the top and the side at an angle (Ti: light blue ("nanoclip"), dark blue (surface); O: red). The end structure of the "nanoclip" is highlighted with yellow oval regions in the top and side views.

gap and corresponds to a large barrier. Fourth, the voltage and the temperature at which the images are recorded are significantly larger than the ones used to observe quantum corral states.

Model

We present here a simple model to compute the STM profiles in the Tersoff-Hamann model for the tunneling probability (18). In the adopted approach, the measured profiles are obtained from the product of the standing wave profiles with the local density of states (LDOS) of the perfect surface along the [001] direction (here perfect means without the end defects). First, we have to compute this defect free LDOS. For this LDOS, we model the system as a one-dimensional box with a background potential which has the $T = 0.295$ nm periodicity of the underlying surface without additional defects. Since the ratio of the amplitudes of short and long period oscillations is observed to be about 1:7, it follows that the defect free LDOS must vary slightly in space with a relative variation of 1:7. To design such a one-dimensional periodic background potential energy (V_{per}), we assume the LDOS spatial variation to be dominated by the spatial dependence of the Bloch wave at the same energy. The electrons are assumed to be confined in the perpendicular direction by the image potential and the bulk band gap, in such as way that only the first energy level corresponding to the well in that direction is involved in the model. In the framework of a perturbative approach, the Fourier coefficients of this Bloch wave (c_g) are proportional to the Fourier coefficients of the potential energy (v_g): $c_g/c_0 = -2mv_g/\hbar^2G^2$. With a sinusoidal shaped Bloch wave, the 1:7 ratio is obtained for $v_1 = -0.31$ eV. So, we may choose a sinusoidal potential energy, $V_{\text{per}} = A\cos(2\pi x/T)$, with an amplitude $A = -0.62$ eV. The band-structure produced by this potential is nearly indistinguishable from that of a free electron with the effective mass of 1.04 times the free-electron mass, except near the band-edge. The 4% difference in effective mass is enough to cause the slight 0.295 nm period oscillation of the defect free LDOS, which would be otherwise strictly constant for a free electron. The local density of states $D_0(r)$ is then given by:

$$D_0(E,x) = \frac{-1}{\pi}\,\text{Im}G_0(E,x,x'),$$

where G_0 is the Green function of the one-dimensional crystal without defects, expressed by

$$G_0(E,x,x') = \sum_{n,k}\frac{\psi_{n\cdot k}(x)\psi^*_{n\cdot k}(x')}{E + i\varepsilon - E_n(k)},$$

where the $\psi_{n,k}$ are the solutions of the Schrödinger equation with the potential V_{per}. Now, we can compute the LDOS for the confined system by adding an explicit potential energy term V_{el} due to the presence of the charged end defects. In Hartree units

$$V_{\text{el}}(x) = \frac{\delta q_1}{L/2 + x} + \frac{\delta q_2}{L/2 - x},$$

where the end defects are separated by a distance L in units of the Bohr radius and carry an effective charge $\varepsilon_r\,\delta q_1$ and $\varepsilon_r\,\delta q_2$ in units of the fundamental charge. This charge is related to the presence of stoichiometric and reduced TiO_2 clusters at the end of the line defects (13). In this form, $\delta q_{1,2}$ implicitly include depolarization effects related to the dielectric constant of inside the nanoclip. The local density of states is computed from the modified Green function of the system using a Dyson equation for adding V_{el} to the one-dimensional Schrödinger equation. The result is the appearance of discrete energy levels. The first energy levels are close to the harmonic oscillator energies which, in Hartree units, are:

$$E_n = E_b + E_{\min} + \left(n + \frac{1}{2}\right)4\sqrt{\frac{\delta q_1 + \delta q_2}{L^3 m^*/m_e}},$$

where E_b is the reference energy (the bottom of the band) taken equal to the chemical potential of the bulk, $E_{\min}$ is the minimum value of V_{el}, m^* is the effective mass of the electrons, and L is the length of the box. The LDOS in the energy range of the first two modes reproduce the spatial characteristics of the observed STM intensity modulation shown in Figs. 1 and 2*A*.

While the above independent-electron model qualitatively describes the formation of the standing wave pattern in the nanoclip, *there is a major qualitative discrepancy between the model and the experiment*. The typical length of the box is about 20 nm and for such a size, the first few energy levels fall inside the thermal energy window available at the temperature at which the oscillations are observed. This means that the experiment should see a mixture of the first states, all with different wavelengths. Consequently, this mixing would wash out the oscillations making them impossible to see. Moreover, the oscillating features have been experimentally proven to be astonishingly robust against the tip bias increasing by up to 0.5 eV. *Clearly there is something fundamentally missing in the simple electron-in-a-box picture*.

In contrast to the reported electron oscillation in a quantum corral on copper, the substrate used in the present study is an insulating material, and there is little or no electronic screening from the bulk material. Also, the electrons are trapped in the box for a long time since there are only a few available surface states through which the confined electrons could leak or escape. The absence of screening and the weakness of the leakage give rise to a charging effect that is due to the presence of electrons that have been injected from the tip. The charging effect makes it much harder to add additional electrons in such a confined space. With the typical dimension of the boxes observed here, we estimate the capacitance of the system to about 10^{-19} F or an equivalent charging energy of about 1.5 eV. The large charging energy can significantly shift and separate the energy levels that are the eigenvalues of the Schrödinger equation. In order to take this effect into account, we have added a self-consistent energy term to our model by including an effective potential obtained by solving the Poisson equation for the electronic density. Since the states and the potential have a mutual dependence, we need to solve a self-consistent problem in order to go beyond the independent-electron picture presented above. Taking electron-electron interaction into account, the one-dimensional Hamiltonian of the system is $H = T + V_{\text{per}} + V_{\text{el}} + V_{\text{sc}}$, where V_{el} is the confining potential energy defined above and V_{sc} is the self-consistent potential energy due to the existing electron density $\rho(x)$. The latter is obtained from Poisson's equation:

$$\Delta V_{\text{sc}}(x) = \frac{-e\rho(x)}{\varepsilon_0},$$

and T is the kinetic energy operator. The one-dimensional electron density is evaluated from

$$\rho(x) = 2e\sum_n |\phi_n(x)|^2,$$

where $\phi_n(x)$'s are the solutions of the Schrödinger equation. The summation is performed on the energy levels up to the tip energy. These levels verify

$$E_n - E_b + \Delta E_n + E_l \le |e|V,$$

where V is the bias potential and ΔE_n's are the contributions of the self-consistent potential to the energy levels. Because the Hamiltonian can be considered in a separable form, the wave function can be expressed as a factor of three functions, corresponding to each direction. It follows that the energy is a sum

of three terms, one for each direction. Here z is normal to the surface and y is normal to the strand defect. For each eigen-energy E_n of the one-dimensional quantum well, there is an infinite number of possible energies E corresponding to the y-dependent wave function solution to the Shrodinger equation, $E = E_n + \frac{\hbar^2}{2m^*}k_y^2$. Because the wave function is confined in the y direction between the two TiO line defects with a separation $D_y = 1.2$ nm, k_y can take on the values $l\pi/D_y$ where l is a positive integer. So the kinetic energy in the y direction is

$$E_l = \frac{\hbar^2}{2m^*}\pi^2 l^2/D_y^2.$$

This method is applied for the analysis of the experimental charge density profiles. The only input to the model is the end charges (δq_1 and δq_2) and the length of the box (L) as shown on Fig. 3*A*. Two examples using the approach described above are included in Fig. 3*B*. The parameters used for these plots where: $L = 14$ nm, $\delta q_1 = 1.22$ e, $\delta q_2 = 0.78$ e, $\mu = 1.8$ eV and $L = 16$ nm, $\delta q_1 = 0.53$ e, $\delta q_2 = 1.9$ e, and $\mu = 1.8$ eV, respectively. Ten other examples of this type of fit are reproduced in the *SI Appendix*. The theoretical line profiles fit closely with the experimental results. It is remarkable that even though the model described here remains relatively simple and elementary,

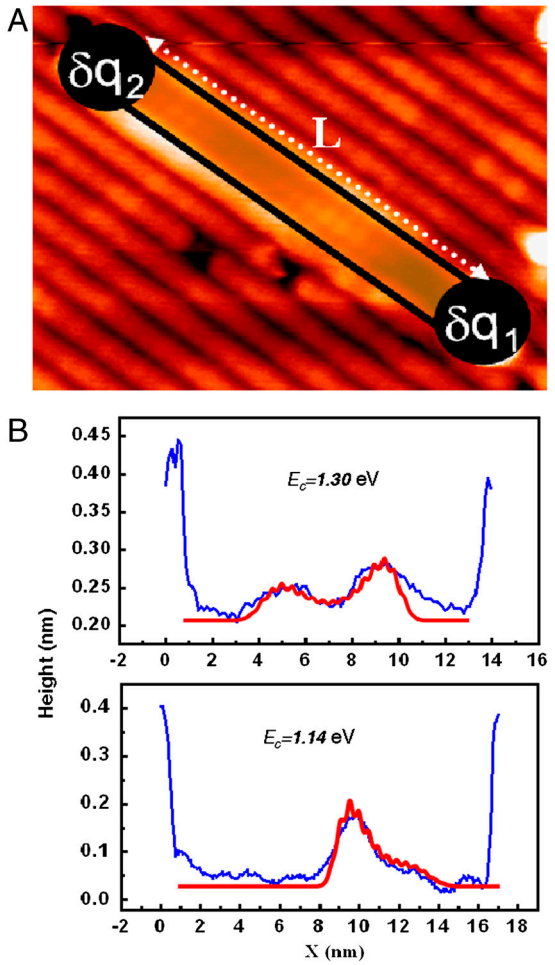

Fig. 3. (*A*) The nanoclip nanostructure can be modeled as a one-dimensional box of length L closed at its ends by two charged structures compatible with the atomistic model shown on Fig. 2*B*. (*B*) Example of how the model, which included electron-electron correlation, can be used to fit the observed (blue) oscillations in the nanoclip. The red curves correspond to the computed charge densities. The calculations indicate that the two examples shown here have a charging energy of 1.3 and 1.14 eV, respectively. (Parameters used: $L = 14$ nm, $\delta q_2 = 0.78$ e and $L = 16$ nm, $\delta q_2 = 1.9$ e, respectively).

it accounts for all the salient features observed in the experiments: position, number, and relative intensity of the peaks, and most importantly their robustness with respect to thermal agitation and change in bias potentials. Recently, Ronnow et al. reported the charge carriers confined to metallic bilayers in $La_{2-2x}Sr_{1+2x}Mn_2O_7$ due to polaron and attributed the STS gap as the energy necessary to dissociate the quasiparticle to extract the electron (hole) from the MnO layer to the tip (19). However in the present study, the observed correlation between the charge density oscillation and the length of the Q1D "box" points to the interference pattern resulting from the Bloch wave functions confined in the box rather than the locally trapped polarons.

We conclude the analysis of the experimental results by a discussion of the number of electrons present in the box. The number of electrons we obtained by our theoretical analysis is not an integer value. In our system, the quantum well communicates with the bulk and the surface. So, the electronic wave function is not entirely localized inside the well. It follows that the integration of the probability density over the quantum well does not yield an integer number. Actually, the charge confinement in this experiment is fundamentally a dynamic process. The electrons come from the tip to the well where they stay a sufficiently long time to produce a charging effect. After that, the electrons tunnel to the bulk or surface states. This tunneling allows a flow of electrons from the tip; otherwise, the STM current would be zero. In our model, for sake of simplicity, we treat the quantum well as an isolated system. We mimic the dynamic behavior by using a noninteger number for the occupation of each level.

Conclusion

We have reported and explained a unique type of "quantum well" grown on an insulating $TiO_2(110)$ surface. The well is effectively closed by the presence of two charged structures at both ends, and they are responsible for a long-range potential that governs the behavior of the electrons inside the well. As expected from a system with quantum confinement, we observe oscillatory features and attribute them to discrete quantum states. The spatial distribution of the charge density fits well with the solution of the Schrödinger equation, provided that correlation effects are included. However, the astounding result is that the charge density distributions are all observed at room temperature and furthermore unchanged within the range of STM tip potential (about 0.5 V variation). Because the substrate is insulating and the electrons are well confined inside the confining structure, the charging-energy-of-a-capacitor model is used to evaluate the corresponding charging energy. Here we find that the system has a very small capacitance of 10^{-19} F corresponding to a charging energy of about 1.5 eV, which is responsible for the robustness of the discrete states with respect to temperature and tip potential. Remarkably, our theoretical analysis indicates that the energy needed to add an extra electron in the two examples shown in Fig. 2 *B*, *C* amounts to 1.30 eV and 1.14 eV for box lengths of 14 nm and 16 nm, respectively. Assuming the capacitance C is proportional to the length of the box and as the charging energy is inversely proportional to the capacitance, these numbers are in excellent agreement with a simple classical picture of capacitor charging, verifying that $E_C(L_1)/E_C(L_2) = L_2/L_1$, independent of the detailed analytical form of the capacitance.

Methods

The experiment was carried out using a variable temperature STM in an ultrahigh vacuum chamber (base pressure < 10^{-10} Torr). A rutile $TiO_2(110)$ sample was cleaned by several cycles of Ar-ion sputtering with the ion current density of about 0.65 μA/cm^2 at the sample for 15–20 min followed by annealing it up to 650 °C for 15 min. A constant current topographic mode was employed for imaging. Sample biases were usually chosen between +1.0 and +2.2 V. All STM images presented here were obtained at room temperature. The surface exhibits a number of linear structures, which look like paperclips,

dispersed on (1×1) terraces Fig. 2*A*. Additional data are presented in the *SI Appendix*.

ACKNOWLEDGMENTS. This research was conducted at the Center for Nanophase Materials Sciences, which is sponsored at Oak Ridge National Laboratory by the Division of Scientific User Facilities, Department of Energy. The present work was also sponsored by the Division of Materials Science, Department of Energy under Contract DEAC05-00OR22725 with UT-Battelle, at Oak Ridge National Laboratory. E.W.P. was supported by DOE #DE-SC0002136. The computations were performed using the resources of the National Center for Computational Sciences at Oak Ridge National Laboratory.

1. Gerber C, Lang HP (2006) How the doors to the nanoworld were opened. *Nat Nanotechnol* 1:3–5.
2. Oncel N, et al. (2005) Quantum confinement between self-organized Pt nanowires on Ge(001). *Phys Rev Lett* 95:116801.
3. Crommie MF, Lutz CP, Eigler DM (1993) Confinement of electrons to quantum corrals on a metal-surface. *Science* 262:218–220.
4. Crommie MF, Lutz CP, Eigler DM (1993) Imaging standing waves in a two-dimensional electron-gas. *Nature* 363:524–527.
5. Nilius N, Wallis TM, Ho W (2002) Development of one-dimensional band structure in artificial gold chains. *Science* 297:1853–1856.
6. Hou JG, et al. (2003) Disorder and suppression of quantum confinement effects in Pd nanoparticles. *Phys Rev Lett* 90:246803.
7. Hou JG, et al. (2001) Nonclassical behavior in the capacitance of a nanojunction. *Phys Rev Lett* 87:049903.
8. Ch Postma HW, Teepen T, Yao Z, Grifoni M, Dekker C (2001) Carbon nanotube single-electron transistors at room temperature. *Science* 293:76–79.
9. Park KT, Pan M, Meunier V, Plummer EW (2006) Surface reconstructions of $TiO_2(110)$ driven by suboxides. *Phys Rev Lett* 96:226105.
10. Zangwill A (1988) *Physics at surfaces* (Cambridge University Press, Cambridge, England).
11. Zhong Q, Vohs JM, Bonnell DA (1992) Effect of reduction on the topographic and electronic structure of $TiO_2(110)$ surfaces. *Surf Sci* 274:35–43.
12. Shibata N, et al. (2008) Direct imaging of reconstructed atoms on TiO_2 (110) surfaces. *Science* 322:570–573.
13. Park KT, et al. (2009) Nanoclusters of TiO_2 wetted with gold. *Surf Sci* 603:3131–3135.
14. Onishi H, Iwasawa Y (1996) Dynamic visualization of a metal-oxide-surface/gas-phase reaction: time-resolved observation by scanning tunneling microscopy at 800 K. *Phys Rev Lett* 76:791.
15. Pang CL, et al. (1998) Added row model of $TiO_2(110)1 \times 2$. *Phys Rev B* 58:1586–1589.
16. McCarty KF (2003) Growth regimes of the oxygen-deficient $TiO_2(110)$ surface exposed to oxygen. *Surf Sci* 543:185–206.
17. Pang CL, Lindsay R, Thornton G (2008) Chemical reactions on rutile $TiO_2(110)$. *Chem Soc Rev* 37:2328–2353.
18. Tersoff J, Hamann DR (1985) Theory of the scanning tunneling microscope. *Phys Rev B* 31:805–813.
19. Ronnow HM, Renner Ch, Aeppli G, Kimura T, Tokura Y (2006) Polarons and confinement of electronic motion to two dimensions in a layered manganite. *Nature* 440:1025–1028.